Small-Angle Neutron Scattering with Contrast Variation Reveals Spatial Relationships between the Three Subunits in the Ternary Cardiac Troponin Complex and the Effects of Troponin I Phosphorylation†

William T. Heller,‡,§ Natosha L. Finley,|| Wen-Ji Dong,⊥ Peter Timmins,# Herbert C. Cheung,⊥ Paul R. Rosevear,|| and Jill Trewhella*,‡

Bioscience Division, Los Alamos National Laboratory, Los Alamos, New Mexico 87545, Department of Molecular Genetics, Biochemistry, and Microbiology, University of Cincinnati, College of Medicine, Cincinnati, Ohio 45267, Department of Biochemistry and Molecular Genetics, University of Alabama at Birmingham, Birmingham, Alabama 35294, and Large Scale Structures Group, Institut Laue-Langevin, Avenue des Martyrs, BP 156 F-38042, Grenoble Cedex 9 France

Received January 27, 2003; Revised Manuscript Received April 22, 2003

ABSTRACT: Small-angle neutron scattering with contrast variation has been used to determine the shapes and dispositions of the three subunits of cardiac troponin and to study the influence of phosphorylation on the structure. Three contrast variation series were collected on three different isotopically labeled variants of the cTnC/cTnI/cTnT(198−298) complex, one of which contained deuterated and bisphosphorylated cTnI. Analysis of the scattering data shows cTnT(198−298) interacting with a single lobe of a somewhat compacted cTnC that sits at one end of an elongated rodlike cTnI, covering about one-third of its length. The cTnT(198−298) sits near the center of the long cTnI axis. The components undergo significant conformational changes and reorientations in response to protein kinase A phosphorylation of cTnI. The rodlike cTnI bends sharply at the end interacting with the cTnC/cTnT(198−298) component, which reorients so as to maintain its contacts with cTnI while undergoing only a relatively small change in shape.

Troponin and tropomyosin form a Ca^{2+}-sensitive switch that regulates the actin-myosin S1 interaction responsible for contraction in striated muscle tissue (for reviews see refs *1*−*4*). Troponin is composed of three subunits; TnC[1] binds Ca^{2+}, TnI inhibits strong contacts between myosin and actin in the absence of the Ca^{2+} signal, and TnT anchors troponin to the thin filament and plays a role in transmitting the Ca^{2+} signal along the thin filament. Two isoforms of TnC and TnI exist in striated muscle; slow skeletal or cardiac (cTnC, cTnI) and fast skeletal (sTnC, sTnI). The isoforms show important structural and functional differences. Unlike sTnC, which has four competent Ca^{2+}-binding sites, cTnC has an inactive Ca^{2+}-binding site (site I) in the regulatory domain (*5*). In the case of TnI, the cardiac isoform has an N-terminal extension with two adjacent serine residues that can be phosphorylated by protein kinase A (PKA) in response to β-adrenergic stimulation (*6*). In mouse cTnI, the 32 residue N-terminal extension has PKA-phosphorylatable serine residues at positions 23 and 24.

The phosphorylation of cTnI is believed to alter the conformational equilibria within the regulatory domain of cTnC, thereby changing the Ca^{2+}-binding behavior of the complex (*7*−*10*). NMR studies indicate that the contacts in the region of the regulatory domain of cTnC and Ser^{23} and Ser^{24} change in response to phosphorylation (*7*, *10*, *11*). FRET studies suggest that the cTnI adopts a more compact conformation when Ser^{23} and Ser^{24} are phosphorylated (*12*, *13*). A surface plasmon resonance study of the complex supports this conclusion (*14*). While such studies establish that the conformation is changing and that contacts between cTnC and cTnI are altered by phosphorylation, they do not reveal the nature of any changes in the global conformations of the protein components.

† This work was performed under the auspices of the U.S. Department of Energy (Contract W-7405-ENG-36) and was supported by the Office of Science/BER project KP1101010 (J.T.) in support of the Oak Ridge Center for Structural Molecular Biology; the National Institutes of Health Grants GM40528 (J.T.), AR44324 (P.R.R.), and HL52508 (H.C.C); and the Department of Defense Grant ARO MURI DAAP19-62-1-0227 (P.R.R.). Neutron scattering data were obtained using instrumentation at the Institut Laue-Langevin.

* Corresponding author. Phone: (505) 667-2690. Fax: (505) 667-2670. E-mail: jtrewhella@lanl.gov.

‡ Los Alamos National Laboratory.

§ Present address: Condensed Matter Sciences Division, Oak Ridge National Laboratory, Oak Ridge, TN 37831.

|| University of Cincinnati.

⊥ University of Alabama at Birmingham.

Institut Laue-Langevin.

[1] Abbreviations: TnC, troponin C; TnI, troponin I; TnT, troponin T; cTnC, recombinant rat cardiac troponin C(des Met^1-Ala^2, Cys35Ser); cTnI, recombinant mouse cardiac troponin I; cTnT(198−298), residues 198−298 of recombinant rat cardiac troponin T; cTnIpp, recombinant mouse cardiac troponin I bisphosphorylated at Ser^{23} and Ser^{24}; Tn_{dC}, cTnC/cTnI/cTnT(198−298) complex having a deuterated cTnC subunit; Tn_{dI}, cTnC/cTnI/cTnT(198−298) complex having a deuterated cTnI subunit; Tn_{dIp}, cTnC/cTnI/cTnT(198−298) complex having a deuterated, bisphosphorylated cTnI subunit at Ser^{23} and Ser^{24}; sTnC, skeletal troponin C; sTnI, skeletal troponin I; sTnT, skeletal troponin T; NMR, nuclear magnetic resonance; FRET, Förster resonance energy transfer; R_g, radius of gyration; d_{max}, maximum linear dimension; AEBSF, 4-(2-aminoethyl)benzenesulfonyl fluoride hydrochloride; BME, β-mercaptoethanol; PMSF, phenylmethylsulfonyl fluoride; DTT, dithiothreitol; ILL, Institut Laue-Langevin; PKA, cAMP-dependent protein kinase A; PCR, polymerase chain reaction.

10.1021/bi0341509 CCC: $25.00
Published on Web 06/04/2003

In our previous small-angle neutron scattering study with contrast variation of the cTnC/cTnI/cTnT(198−298) complex with deuterated cTnC (Tn_{dC}) (*15*), we identified significant structural differences between the isoforms of the cardiac subunits and those of skeletal troponin. Earlier neutron scattering experiments of the skeletal system (*16*) revealed that sTnC is extended in the ternary skeletal troponin complex, as it is in the binary sTnC/sTnI complex (*17*, *18*) and in the crystal structure of the isolated sTnC that first revealed its distinctive dumbbell shape (*19*). In contrast, our neutron scattering studies of cardiac troponin revealed a partially collapsed conformation for cTnC in which the two Ca^{2+}-binding lobes are in closer proximity (*15*). This result is supported by NMR studies of cTnC complexed with cTnI (*20*). The crystal structure of sTnC complexed with the peptide sTnI(1−47) also reveals a partially collapsed conformation for sTnC (*21*), although the orientation of the globular lobes with respect to each other differs, suggesting that TnC's inherent potential for flexibility is an important consideration in interpreting structural data and in understanding the details of its function as a molecular switch. Neutron scattering studies also revealed that sTnI in the binary complex (*17*, *18*) and in the ternary troponin (*16*) is even more extended than isolated sTnC (*20*), although additional interactions with sTnT appear to stabilize a somewhat more compact version as compared to the binary complex. In the binary complex, sTnC and sTnI are highly intertwined (*17*, *18*, *22*), while cTnC and cTnI/cTnT(198−298) have a much smaller surface area of interaction (*15*).

In this paper, we present the results of experiments using small-angle neutron scattering with contrast variation to study three variants of cardiac troponin. We repeated our measurements on the Tn_{dC} complex (*15*). To obtain more information on the organization of the subunits within the unphosphorylated complex, we also collected data on the same complex but with cTnI deuterated (Tn_{dI}), which allowed us to determine the shape of the cTnI component within the ternary complex and infer the location and shape of cTnT(198−298). We also evaluated the effects of PKA phosphorylation by collecting data for the complex with cTnI both deuterated and phosphorylated (Tn_{dIp}). All of these experiments were done using samples in which the complexes were Ca^{2+}-saturated.

MATERIALS AND METHODS

Troponin Complex Formation. [^{15}N, D]cTnC and cTnI were expressed and purified as previously described (*7*). cDNA encoding of cTnT(198−298) was generated by PCR and subcloned into the pET23d$^+$ expression vector. cTnT(198−298) was expressed in BL21(DE3)-RIL cells and purified by chromatography on Pharmacia CM-Sepharose and Superdex 75 columns. Complex formation was carried out by dissolving cTnC, cTnI, and cTnT(198−298) at a molar ratio of 1:1:1.1 in 6 M urea, 150 mM NaCl, 25 mM Tris (pH = 7.5), 1 mM EDTA, 1 mM DTT, and 1 mM PMSF. An extensive dialysis against 25 mM Tris (pH = 7.5), 10 mM BME, 10 mM DTT, 10 mM $CaCl_2$, 0.1 mM AEBSF, and 0.1 mM leupeptin followed. Complex formation was monitored by following individual [^{15}N, D]cTnC amide resonances in H-^{15}N HSQC NMR spectra. NMR samples of Ca^{2+}-saturated [^{15}N, D]cTnC/cTnI/cTnT(198−298), 0.4−1.0 mM, were prepared by exchanging [^{15}N, D]cTnC/cTnI/cTnT(198−298) into buffer containing 10% D_2O, 20 mM Tris-d_{11} (pH = 6.8), 500 mM KCl, 10 mM $CaCl_2$, 5 mM DTT, 5 mM BME, 0.1 mM AEBSF, and 0.1 mM leupeptin. If necessary, the [^{15}N, D]cTnC/cTnI/cTnT(198−298) complex was further purified by size exclusion chromatography on a Pharmacia Superdex 75 column equilibrated in 20 mM Tris (pH = 7.5), 500 mM KCl, 10 mM $CaCl_2$, 5 mM BME, and 1 mM PMSF. Preparation of the complexes with the deuterated cTnI component were formed in a similar fashion (*7*).

Phosphorylation of cTnI. cTnI was phosphorylated by the catalytic subunit of PKA, using a cTnC affinity column as previously described (*11*). In this procedure, the phosphorylation was carried out in the column for 20 min at 30 °C, and the reaction was terminated by washing the column with cold buffer containing Ca^{2+}. Phosphorylated cTnI was eluted with buffer containing EDTA. The extent of phosphorylation was quantified by treatment of the sample with alkaline phosphatase, followed by determination of inorganic phosphate using the EnzChek Phosphate Assay kit. Phosphorylation of the two PKA sites in cTnI was >90%.

Preparation of Stock Solutions for Neutron Scattering. H_2O and D_2O Buffer solutions were prepared containing 20 mM Tris, 500 mM KCl, 10 mM $CaCl_2$, 5 mM DTT, and 0.1 mM AEBSF. The solutions were titrated to a final pH of 7.5 with either HCl or DCl. Equal aliquots (∼1 mL) of the original stock solutions of the three complexes were dialyzed overnight against either the H_2O or the D_2O buffers using a dialysis membrane with an 8 kDa molecular mass cutoff. The original complex concentrations were 3.5−5.8 mg/mL. For more accurate background subtraction, quantities of each dialysate from the dialyses were retained for use in the neutron scattering experiments.

Small-Angle X-ray Scattering Measurements. Small-angle X-ray scattering measurements were performed with the line source instrument at Los Alamos National Laboratory (*23*). Data reduction followed published procedures to correct for detector sensitivity and background signal (*23*). The measurements also served to determine that the samples were free from nonspecific aggregation and the influence of interparticle interference. Because X-rays are scattered by electrons, the different isotopic compositions of the components in the complex do not effect the scattering densities. The data can be used to produce models of the overall complex assuming it is a uniform scatterer with internal density fluctuations significantly less than the contrast (the square of the scattering length density difference) between the complex and the solvent. The monodispersity of the sample was characterized by collecting data at a series of fractional protein concentrations (c) of 1.0, 0.8, 0.6, 0.4, and 0.2 of the complex in the H_2O and D_2O stock solutions. To determine protein concentration, data were collected for a lysozyme standard (*24*) at the same fractional concentrations to calibrate the $I(0)$ values, which are related to the molecular weight of the protein through the equation $I_{lys}(0)/m_{lys}c_{lys} = I_{tn}(0)/m_{tn}c_{tn}$ (lys = lysozyme, tn = troponin, m = molecular weight, and c = concentration in mg/mL).

Small-Angle Neutron Scattering Measurements. Mixtures of the H_2O and D_2O stock sample solutions were made with 0, 10, 20, 30, 40, 90, and 100% of the D_2O stock solution in preparation for measuring seven different neutron contrast values (see *Data Analysis* section). Corresponding back-

ground solutions were made. All volumes for mixing were weighed to ensure optimal background subtraction for the samples in the data reduction. The 0, 10, 20, 30, and 40% samples were measured using 1 mm path length cells, while 2 mm path length cells were used for the 90 and 100% samples. The precise D_2O content of each solution was determined by comparing its neutron transmission to that of the H_2O buffer and pure D_2O. The transmission, T, is related to the absorbance, μ, and path length, d, of the sample by $\mu = \ln(T)/d$. The absorbance varies linearly with hydrogen content of the buffer. The results of the hydrogen content determination were used throughout the analysis of the data, but the percentage mixtures for the H_2O/D_2O solutions are given as unadjusted numbers representing the mixing of the stock solutions throughout this paper.

Small-angle neutron scattering experiments were performed at the High-Flux Reactor of the Institute Laue-Langevin in Grenoble, France using the D-22 SANS instrument (*25*). Two instrument settings were used to provide an adequate q range for the data analysis (0.01−0.30 $Å^{-1}$); detector distance 4 m and wavelength 10 Å for low q and detector distance 2.5 m and wavelength 5 Å for high q data. The wavelength spread was $\Delta\lambda/\lambda = 0.10$ (fwhm). Sample and background intensities were collected at both instrument settings for all samples. Data reduction followed standard procedures (*26*) to correct for detector sensitivity and sample background. The data sets from the two distances were merged using the routines included with the data reduction software. Errors cited for parameters are propagated from the counting statistics of the scattering data.

Small-Angle Scattering Data Analysis. The small-angle scattering intensity profile of monodisperse, identical particles in solution can be written as

$$I(q) = |\langle \int_V (\rho(\vec{r}) - \rho_s) e^{-i\vec{q}\cdot\vec{r}} d^3r \rangle|^2 \quad (1)$$

where $\rho(\vec{r})$ is the scattering length density of the particle, and ρ_s is the average scattering length density of the solvent. $\vec{q}$ is the momentum transfer, having the magnitude $4\pi(\sin\theta)/\lambda$, where 2θ is the scattering angle and λ is the wavelength. The integration over the particle volume is rotationally averaged. The experiment measures the time and ensemble average information for all particles in solution.

Small-angle scattering data can be analyzed according to Guinier analysis to give an estimate of R_g (*27*). The probable distribution of vector lengths, r, between scattering centers within the scattering object, $P(r)$, provides more information on the shape. The relationship between $I(q)$ and $P(r)$ is given by the Fourier transform in eq 2.

$$P(r) = \frac{1}{2\pi^2}\int_0^\infty dq(qr)I(q)\sin(qr) \quad (2)$$

The indirect Fourier transform algorithm developed by Moore (*28*) was used to determine $P(r)$ from the measured intensity profile. An expansion in $\sin(qr)/qr$ is used to describe the intensity profiles. The boundary conditions $P(r)/r = 0$ at $r = 0$ and d_{max} are applied to $P(r)$.

Contrast variation is a powerful tool for studying proteins in solution. Neutrons are scattered by atomic nuclei, and as a result isotopes of the same element can have very different neutron scattering properties. The dramatic difference in the scattering lengths of hydrogen and deuterium makes it possible to change the scattering length density of a protein by substituting one isotope for the other. Small-angle neutron scattering data for a sample containing one component labeled with deuterium and another unlabeled component can be collected in several H_2O/D_2O mixtures to give a contrast series of measurements of intensity profiles, $I(q)$. These $I(q)$ versus q data sets can be written as a set of linear equations in the basic scattering functions corresponding to the scattering functions of the labeled and unlabeled components and a cross-term (*17*, *29*). The Fourier transform of the cross-term gives the distribution of vectors lengths between the labeled and the unlabeled components. A multiple linear regression routine (*30*) was implemented in the C programming language at Los Alamos National Laboratory to solve for the three basic scattering functions from the contrast series. These basic scattering functions are then used to derive information on the shapes of the components, as well as their relative dispositions.

Structural models of the isotopically labeled subunits and the overall complex were determined from the basic scattering functions and the X-ray scattering data using methods developed at Los Alamos National Laboratory. The same modeling approaches were employed to generate models in this study as were used in our earlier studies of cardiac troponin (*15*): GA_STRUCT is a program that generates ab initio shapes to fit scattering data, while CONTRAST uses the contrast series data to determine the relative positions and orientations of components using the shapes found by GA_STRUCT. GA_STRUCT produces a family of models composed of aggregates of spheres that fit the intensity profile. The family of structures is then characterized for similarity to produce a consensus envelope representing the portions of structure that are consistent across the majority of the members of the family of structures. CONTRAST takes a set of known structures and finds the relative position and orientation of the structures that best fits a set of contrast variation intensity profiles. Both GA_STRUCT and CONTRAST use the fitting parameter F defined in eq 3 to evaluate the quality of the fit.

$$F = \frac{1}{N_{pts}}\left(\sum_{N_{pts}} \frac{(I(q) - I_m(q))^2}{\sigma(q)^2}\right) \quad (3)$$

N_{pts} is the number of points in the data set, $I(q)$ and $I_m(q)$ are the experimental and model intensities, respectively, and $\sigma(q)$ is the experimental uncertainty of $I(q)$.

RESULTS

Table 1 shows the R_g and d_{max} values determined from the small-angle X-ray scattering data collected for the lysozyme standard and the three troponin complexes collected in H_2O and D_2O. The protein concentrations in the stock solutions, determined as described in Materials and Methods, are included in Table 1 for reference. These concentration values were used in the extraction of the basic scattering functions. Figure 1 shows a plot of the $P(r)$ functions of the unphosphorylated (Tn_{dI} in H_2O is shown) and phosphorylated (Tn_{dIp} in H_2O is shown) troponin complexes determined from the X-ray scattering data. The curve for the unphosphorylated complex clearly has a rodlike

Table 1: Structural Parameters Derived from the X-ray Scattering Data for Lysozyme and the Troponin Complexes in H_2O and D_2O as Determined by $P(r)$ Analysis Using the Moore Algorithm (*28*)[a]

	R_g (Å)	d_{max} (Å)	c (mg/mL)
lysozyme standard in H_2O (*24*)	14.6 ± 0.3	45 ± 2	infinite dilution
Tn_{dC} H_2O	30.3 ± 1.3	96 ± 7	4.1
Tn_{dC} D_2O	29.2 ± 1.0	90 ± 5	4.6
Tn_{dI} H_2O	31.7 ± 1.3	95 ± 5	3.7
Tn_{dI} D_2O	28.7 ± 1.3	90 ± 6	3.5
Tn_{dIp} H_2O	31.3 ± 1.7	100 ± 6	3.9
Tn_{dIp} D_2O	31.9 ± 0.9	97 ± 5	5.8

[a] The R_g and d_{max} values for the Tn_{dC} in H_2O are smaller, by ~3 and 4 Å, respectively, than determined from our earlier measurements of this complex (*15*). From Table 2, it can be seen that this difference is attributable to differences in the cTnI/cTnT(198−298) component. The results of the lysozyme measurements, which were determined from data extrapolated to infinite dilution, and the resulting troponin complex concentrations are included for reference.

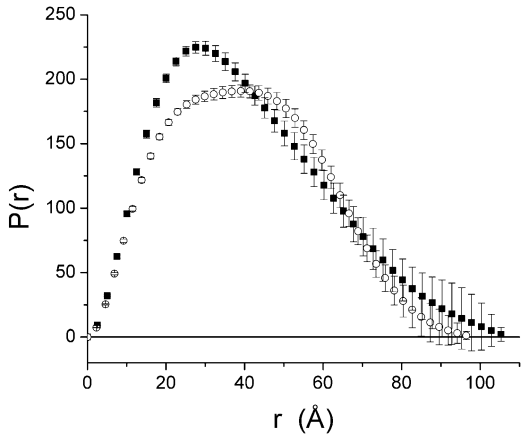

FIGURE 1: $P(r)$ functions derived from the X-ray scattering data using Moore's algorithm (*28*). The Tn_{dI} complex in H_2O (■) and the TndIp complex in D_2O (○) are shown.

character with peak near 27 Å and a very weak shoulder near 50 Å. The $P(r)$ for the phosphorylated complex has a single broad peak that is centered around 35 Å indicating a significant change in the overall conformation of the troponin complex upon phosphorylation.

The scattering data from the three neutron contrast variation series collected are plotted in Figure 2; top is Tn_{dC}, middle is Tn_{dI}, and bottom is Tn_{dIp}. There are only six complete intensity profiles for the phosphorylated complex because data were only collected at 4 m for the 100% D_2O sample. The inset plots are of $\sqrt{I(0)}$ versus the fraction of D_2O in the solvent, determined from the sample transmissions. The $I(0)$ values were corrected for protein concentration and sample path length. All three curves are fit well with a straight line. The x intercept (%D_2O) is the contrast match point for the complex, which is used to determine the level of deuteration of the labeled subunits. The Tn_{dC} complex was deuterated to ~91% of all nonexchangeable hydrogens, while the Tn_{dI} and Tn_{dIp} complexes were deuterated to ~75%.

Stuhrmann plots (*17*, *29*) for each contrast variation series are shown in Figure 3. The square of the R_g determined from the intensity profiles in the series are plotted as a function of the inverse of the contrast of the complex. This curve can be described as a quadratic form, the coefficients of

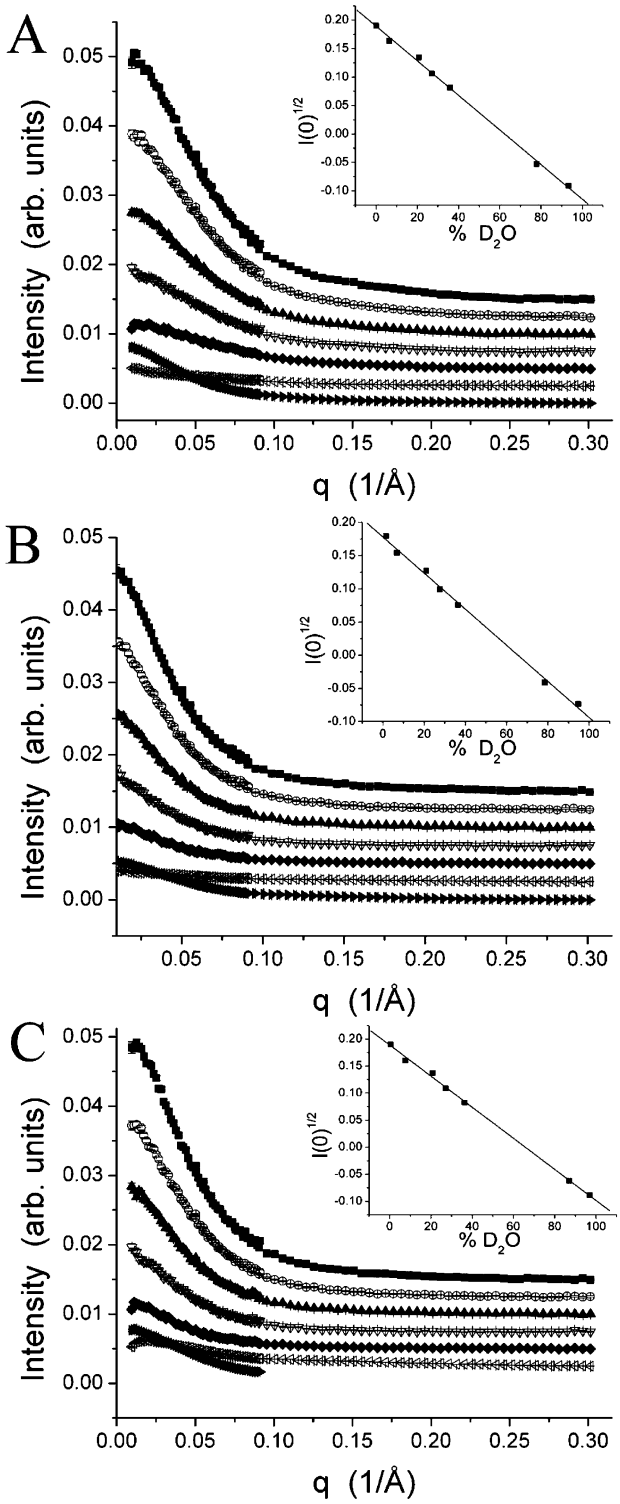

FIGURE 2: Neutron contrast variation series for the three troponin complexes measured: (A) Tn_{dC}, (B) Tn_{dI}, and (C) Tn_{dIp}. The intensity profiles have been vertically offset for clarity. Each symbol corresponds to a %D_2O in the solution from top to bottom: ■ (0%), ○ (10%), ▲ (20%), ▽ (30%), ◆ (40%), open triangle pointing left (90%), and solid triangle pointing right (100%). The inset plots are of vs %D_2O. The x intercept shows the contrast match point for the complex.

which can be related to the R_g of the components and the approximate separation of the centers of mass. The Tn_{dC} curve has a clear quadratic character. Analysis of the curvature indicates that the centers of mass of the cTnC and cTnI/cTnT(198−298) are separated by 34 ± 4 Å. The curve

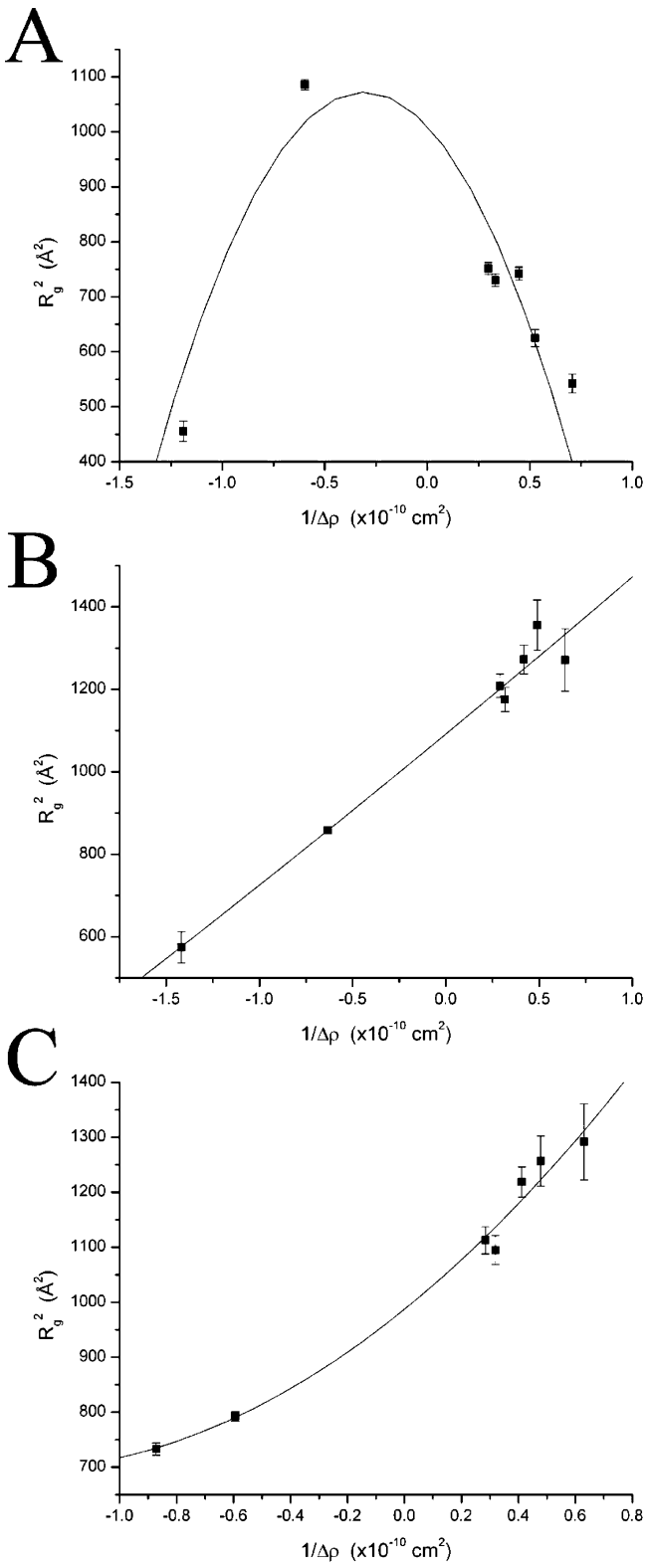

FIGURE 3: Stuhrmann plots (*18*, *29*) for Tn_{dC} (A), Tn_{dI} (B), and Tn_{dIp} (C).

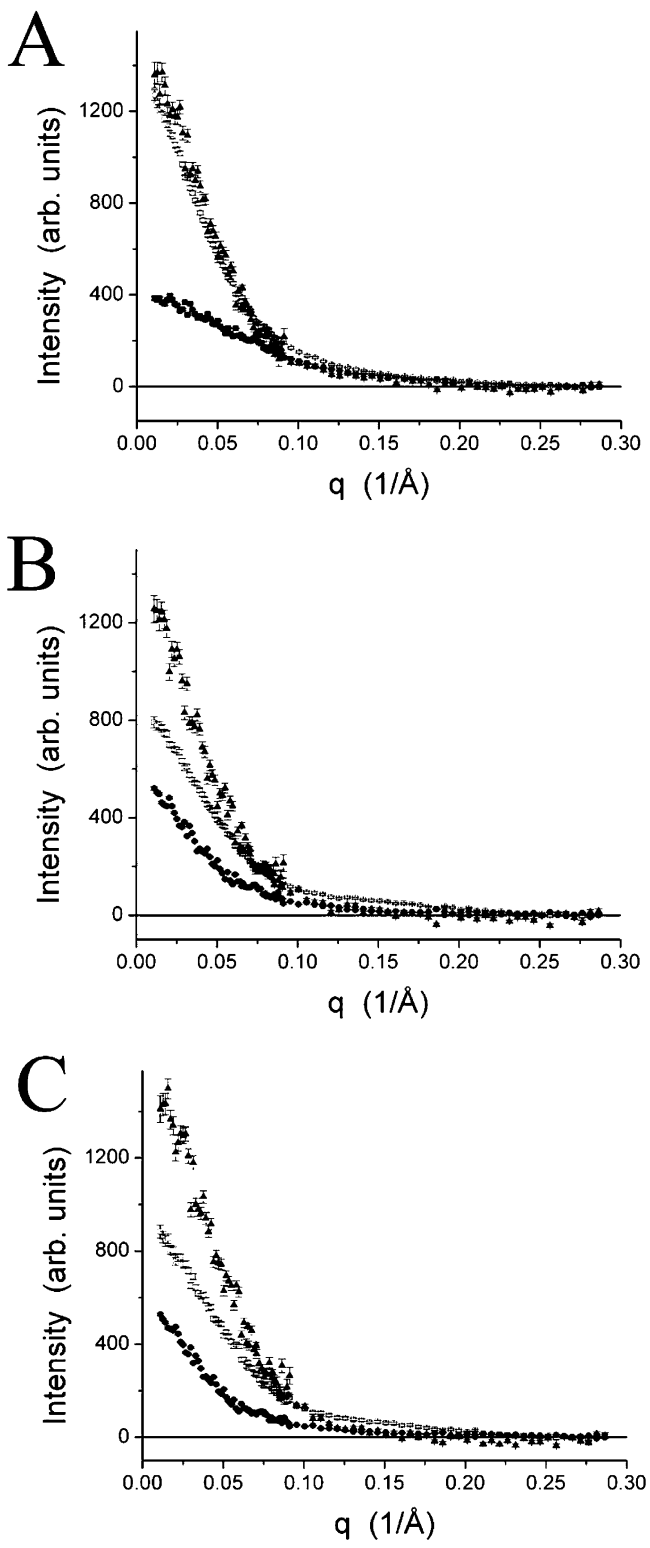

FIGURE 4: Basic scattering functions for Tn_{dC} (A), Tn_{dI} (B), and Tn_{dIp} (C). The curves in each plot are the deuterated component (●), the undeuterated component (□), and the cross-term (▲).

fit to the data of the Tn_{dI} complex is almost a straight line, having a very slight positive curvature. The fit indicates that the centers of mass of the cTnI and the cTnC/cTnT(198−298) are nearly coincident (<10 Å). The positive curvature for Tn_{dIp} could be indicative of inhomogeneous labeling of the deuterated subunit (*31*) or be the result of slight D_2O-induced aggregation, although there was no clear evidence for aggregation. Inhomogeneous labeling could be the result of differential exchange mechanisms in cTnI caused by phosphorylation. Inhomegeneity in the labeling would affect all the Stuhrmann analyses, resulting in the calculated separation of the centers of mass being systematically small.

The basic scattering functions extracted from the three contrast series are shown in Figure 4. The results for the Tn_{dC} complex (Figure 4A) reproduce the results from the basic scattering functions of the previous neutron scattering

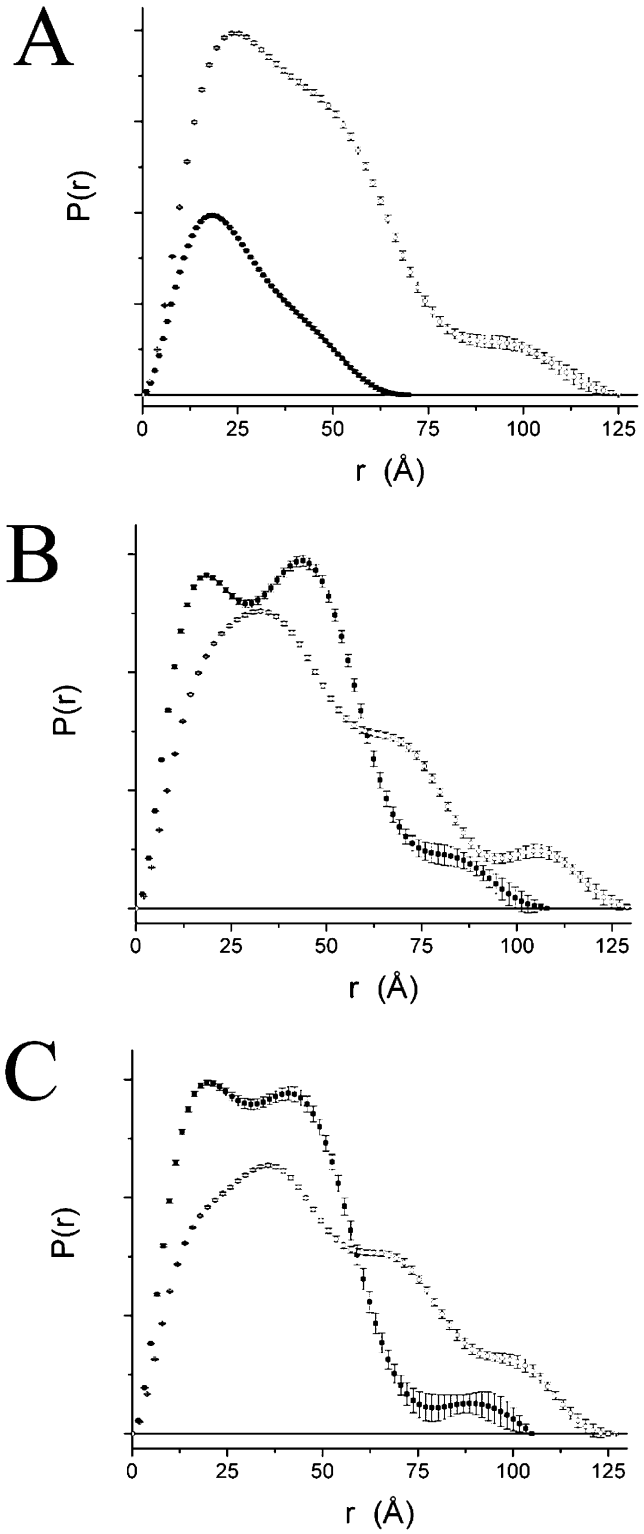

FIGURE 5: *P*(*r*) functions derived from the basic scattering functions for Tn_{dC} (A) (cTnC ■, cTnI/cTnT(198−298) ○), Tn_{dI} (B) (cTnC/cTnT(198−298) ■, cTnI ○), and Tn_{dIp} (C) (cTnC/cTnT(198−298) ■, cTnI ○).

experiment very well (*15*). The *P*(*r*) for the cTnC component (Figure 5A) agrees with the previous experiment to within error, while there are small differences in the *P*(*r*) for the cTnI/cTnT(198−298) component between the experiments, which is also reflected in somewhat smaller R_g and d_{max} values (see Tables 1 and 2 and Discussion). The curves for the Tn_{dI} and Tn_{dIp} complex both indicate a highly extended

Table 2: Structural Parameters of the Troponin Complex and Isotopically Labeled Components as Determined by *P*(*r*) Analysis Using the Moore Algorithm (*28*)[a]

	R_g (Å)	d_{max} (Å)
cTnC	20.1 ± 0.1	70 ± 3
cTnI/cTnT(198−298)	33.3 ± 0.4	125 ± 6
cTnI	38.0 ± 0.3	131 ± 5
cTnC/cTnT(198−298)	29.6 ± 0.5	108 ± 8
cTnIpp	39.0 ± 0.3	127 ± 7
cTnC/cTnT(198−298) (phos.)	28.3 ± 0.6	105 ± 8
cTnC (*15*)	20.1 ± 0.7	65 ± 5
cTnI/cTnT(198−298) (*15*)	35.0 ± 1.4	115 ± 8
cTnC/cTnI/cTnT(198−298) (*15*)	33.1 ± 0.5	100 ± 5

[a] Structural parameters determined in the previous small-angle scattering study of the Tn_{dC} are provided for comparison (*15*). Note that the cTnI/cTnT(198−298) component has a smaller R_g and d_{max} value as compared to what was previously measured, while the values for cTnC are unchanged.

Table 3: Structural Parameters for the Consensus Envelopes Produced by GA_STRUCT from the Basic Scattering Functions

	R_g (Å)	d_{max} (Å)
cTnC	20.6	70.6
cTnI/cTnT(198−298)	34.4	123.4
cTnI	30.5	99.1
cTnC/cTnT(198−298)	39.0	137.9
cTnIpp	28.8	93.5
cTnC/cTnT(198−298) (phos.)	40.5	141.5

structure, but the *P*(*r*) functions determined from the basic scattering functions of the three complexes (Figure 5B,C) reveal significant differences. *P*(*r*) functions for cTnC/cTnT-(198−298) (Figure 5B,C) show two strong peaks at ∼18 and 45 Å, but the ratio of the peak heights varies with the second peak weakening upon phosphorylation. At the same time, the broad peak around 25 Å of the *P*(*r*) for the cTnI component resolves into a peak at 30 Å and a shoulder at ∼12 Å upon phosphorylation. There is also an increase in the relative intensity of the vector lengths >50 Å. It may be relevant that cTnI is predicted to be a mostly α-helical protein, and the shoulder at 12 Å that is most evident in the phosphorylated state could be due to this large amount of α-helix. The R_g and d_{max} values calculated from the *P*(*r*) functions of the basic scattering functions are listed in Table 2. The effects of phosphorylation of cTnI is seen in a decrease in R_g for cTnI by 1 Å and a corresponding increase for cTnC/cTnT(198−298) by 1.3 Å.

Figure 6 shows the results of shape restoration by GA_STRUCT applied to the X-ray scattering data of the Tn_{dI} and Tn_{dIp} complexes. The unphosphorylated complex can be reasonably approximated by a peanut shape. The length of the envelope is ∼108 Å, and the width is ∼50 Å. In contrast, the Tn_{dIp} structure is a bent rod. The length of the envelope is ∼104 Å, and the width of each globular domain is ∼40 Å. The R_g and d_{max} of the consensus envelopes are listed in Table 3.

The results of GA_STRUCT shape restoration applied to the basic scattering functions are shown in Figures 7−9 (Tn_{dC}, Tn_{dI}, and Tn_{dIp}, respectively). Each consensus envelope is shown in three orthogonal views, and the structural parameters of the consensus envelopes are listed in Table 3. The consensus envelopes for the Tn_{dC} (Figure 7) reasonably

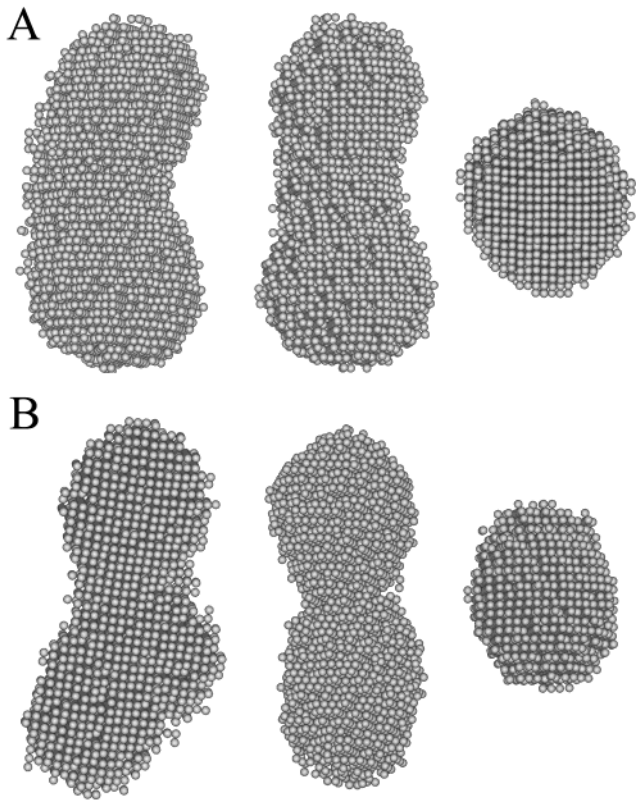

FIGURE 6: Three orthogonal views of the consensus envelopes produced by GA_STRUCT from the X-ray scattering intensity profiles for the unphosphorylated (A) and phosphorylated (B) troponin complex.

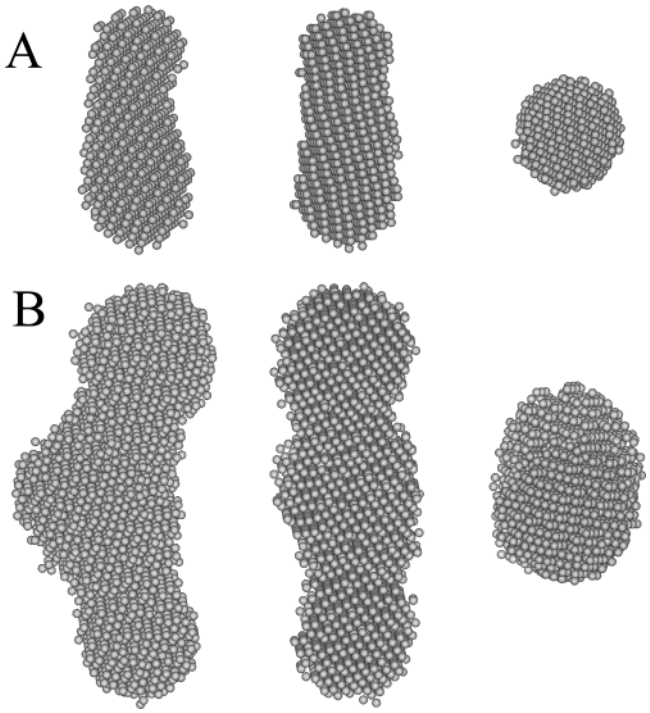

FIGURE 7: Three orthogonal views of the consensus envelopes produced by GA_STRUCT from the Tn_{dC} basic scattering functions: cTnC (A) and cTnI/cTnT(198−298) (B).

reproduce the results of the previous neutron scattering study of the complex (*15*). The cTnC component is a relatively compact structure with indications that it is bilobal. The results of applying CONTRAST to the cTnC basic scattering

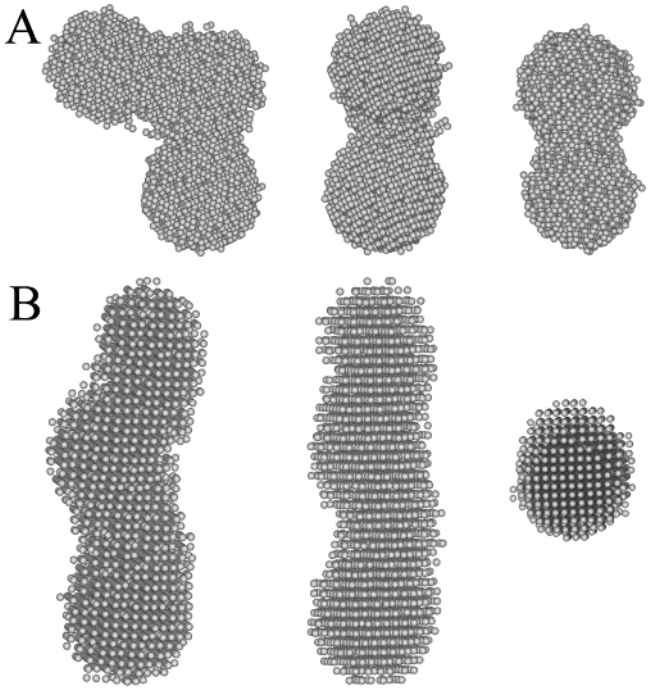

FIGURE 8: Three orthogonal views of the consensus envelopes produced by GA_STRUCT from the Tn_{dI} basic scattering functions: cTnC/cTnT(198−298) (A) and cTnI (B).

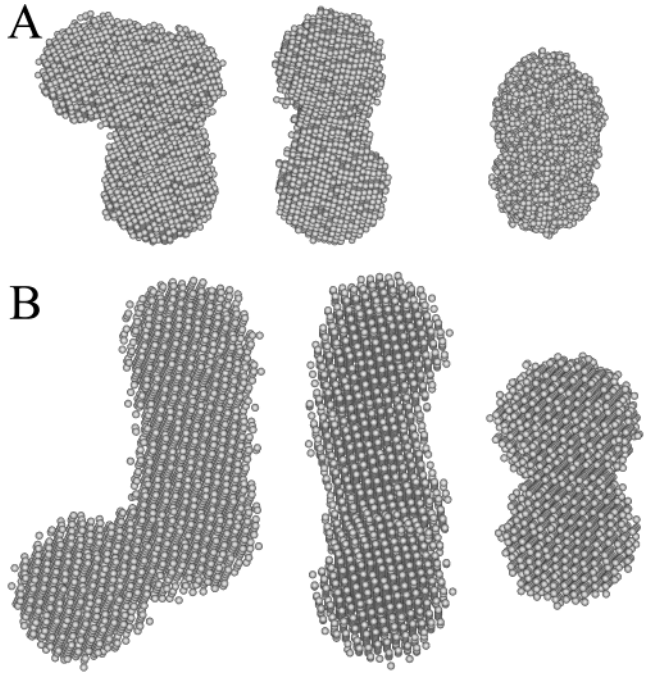

FIGURE 9: Three orthogonal views of the consensus envelopes produced by GA_STRUCT from the Tn_{dIp} basic scattering functions: cTnC/cTnT(198−298) (A) and cTnI (B).

function using the NMR structure (*20*) reproduce the results presented in the previous study (*15*) in that the cTnC structure is partially collapsed and thus are not presented again here. The cTnI/cTnT(198−298) component is an extended, rodlike structure with a slight bend near the middle.

The structures determined from the basic scattering functions of the Tn_{dI} (Figure 8) and Tn_{dIp} (Figure 9) complexes are also rodlike but with distinctive differences. The cTnI has a rodlike structure with some bulges in both the phosphorylated and the unphosphorylated forms, and phos-

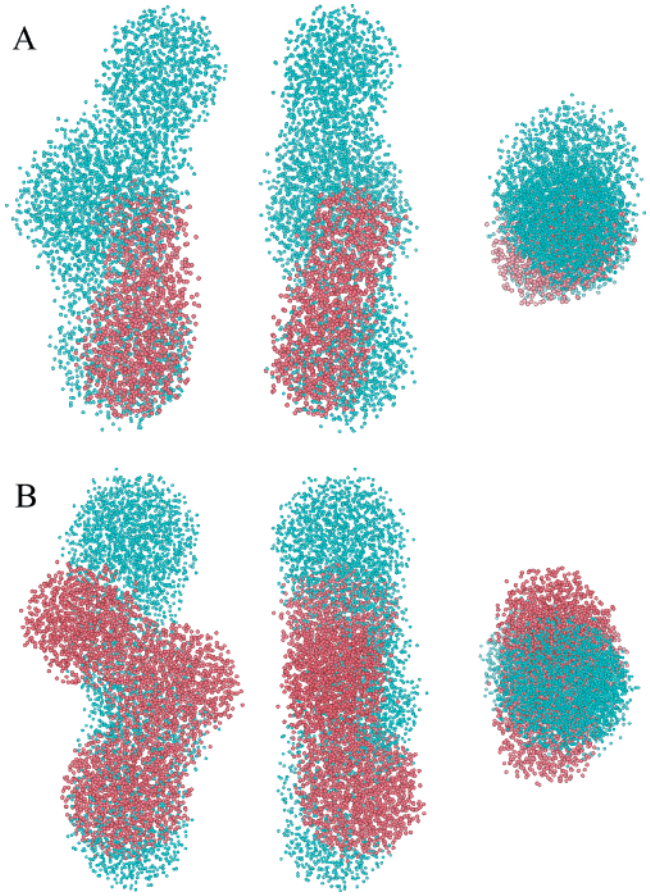

FIGURE 10: Three orthogonal views of the structures produced by CONTRAST by modeling against the contrast variation series using the consensus envelopes derived from the basic scattering functions for the Tn_{dC} (A) and Tn_{dI} (B) complexes. The cTnC in Tn_{dC} and the cTnC/cTnT(198−298) in Tn_{dI} are colored red.

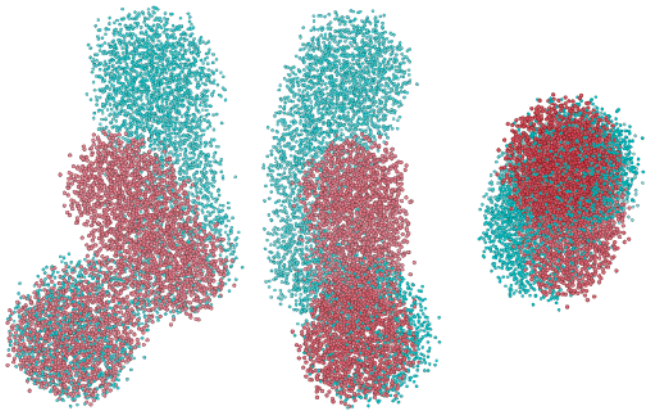

FIGURE 11: Three orthogonal views of the structure produced by CONTRAST for Tn_{dIp}. The cTnC/cTnT(198−298) in Tn_{dIp} is colored red.

phorylation causes the cTnI to bend at one end. Both of the cTnC/cTnT(198−298) components are L-shaped structures made up of two or three ellipsoidal domains, although the L-shape and possible three domain structure is more accentuated in the nonphosphorylated complex.

Models of the intact complex were developed using the consensus envelopes produced by GA_STRUCT and the contrast variation series for all three sets of intensity profiles. The models produced by CONTRAST of the two unphosphorylated troponin complexes are shown in Figure 10 in three orthogonal views. The Tn_{dC} model (Figure 10A) has

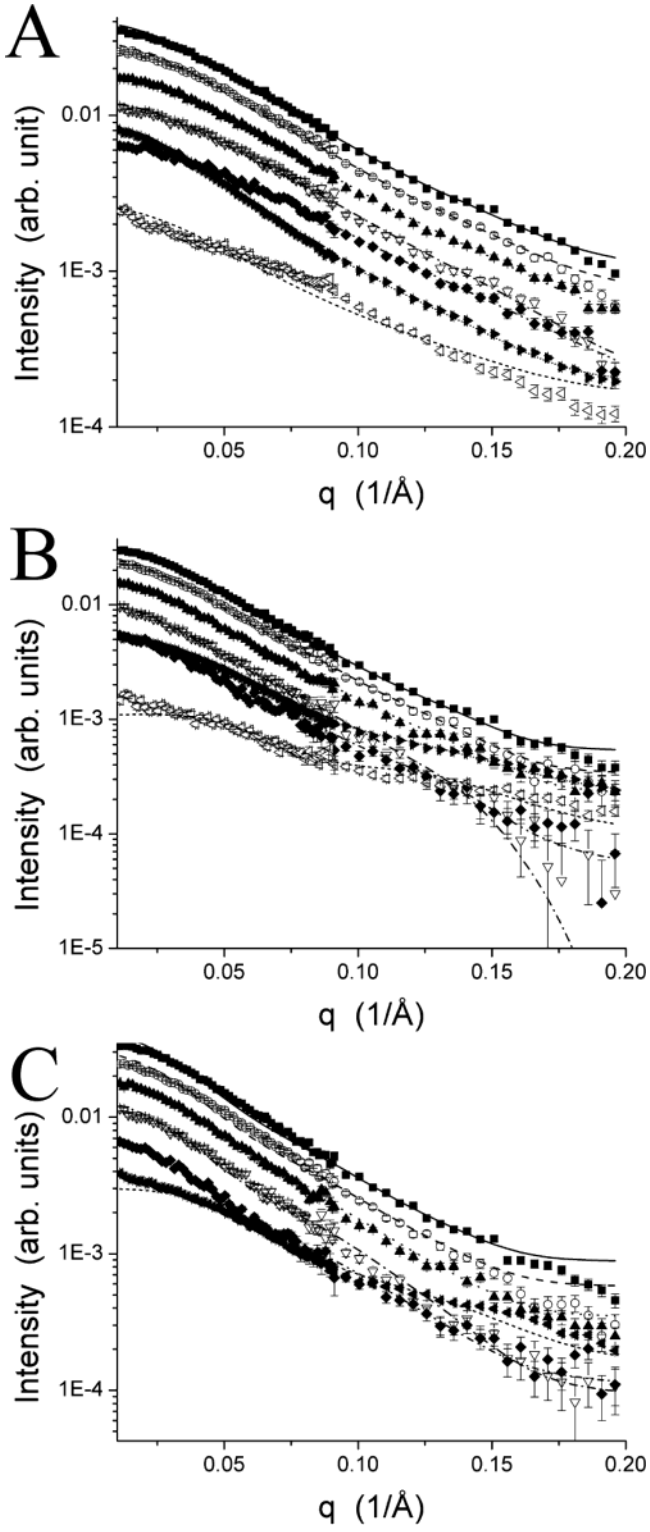

FIGURE 12: Fit of the model intensities produced by contrast to the series data for Tn_{dC} (A), Tn_{dI} (B), and Tn_{dIp} (C). The %D2O solutions are labeled as follows from top to bottom: ■ and solid line (0%), ○ and dashed line (10%), ▲ and dotted line (20%), ▽ and dash−dot line (30%), ◆ and dash−dot−dot line (40%), open triangle pointing left and short dash line (90%), and closed triangle pointing right and fine dotted line (100%). The 100% plot is missing from the Tn_{dIp} series because it was incomplete.

the cTnC component lying roughly parallel to the long axis of the cTnI/cTnT(198−298) component. The volume for which the components overlapped in the model is attributed to cTnC because this assignment gave a significantly better

fit to the data than assigning it to cTnI/cTnT(198−298). The overall structure of the Tn_{dI} complex (Figure 10B) is very similar to that of the Tn_{dC} complex. The peanut-shaped domain of the cTnC/cTnT(198−298) component overlays well with the cTnC component from the other structure. The position and shape of cTnT(198−298) can be inferred to be the extra globular domain located near the center of the cTnI component, which appears as the shoulder on the cTnI/cTnT-(198−298) consensus envelope from the Tn_{dC} results (Figure 7B). The models indicate that the cTnT(198−298) interacts with only one Ca^{2+}-binding domain of the cTnC (Figure 10) but cannot be used to say which domain. The model of the phosphorylated complex produced by CONTRAST using the cTnC/cTnT(198−298) and cTnIpp envelopes is shown in Figure 11. Phosphorylation of cTnI results in a rotation of cTnC and the segment of cTnI interacting with it away from the axis of the original cylinder.

The fit of the model intensities to all three contrast variation series are shown in Figure 12. The fitting parameters for the final models were 5.8 (Tn_{dC}), 2.8 (Tn_{dI}), and 14.2 (Tn_{dIp}). An F value of 1.0 implies that the model intensity fits the data and that the counting statistics of the data are representative of the errors in the data. The fact that our values of the fit parameter are greater than 1.0 is most likely attributable to the high statistical quality of the ILL data that results in statistical uncertainties that are not representative of the true errors. The higher fit value for the Tn_{dIp} series might also in part be attributed to the inhomogeneous labeling of the components that is suggested by the Stuhrmann plot, which would result in poor fits at high q values where the effects of internal density fluctuations can be apparent. Another possible cause of the difficulties in fitting the contrast variation series for the phosphorylated sample could be the effects of interparticle interference, suggested by the slight downturn at low q in the Tn_{dIp} data (Figure 12C). Phosphorylation causes the complex to become more negatively charged, which can result in an increased tendency for spatial correlations between the particles in solution. Although we saw no evidence for this effect in our X-ray measurements, to ensure that possible interparticle interference effects were not impacting our modeling results, the modeling was repeated with a higher cut off for the low q data, and the results were not affected.

DISCUSSION

This study of the cardiac troponin with a new sample preparation and greatly improved statistics in our scattering data has confirmed our previous observations (*15*). The cTnC component is somewhat compacted and interacts with an approximately rod-shaped cTnI/cTnT(198−298) component with the area of interaction centered roughly one-third of the way along the rod. Some differences to the previous experiment were noted. The cTnI/cTnT(198−298) component is somewhat straighter and smaller than previously determined (by ∼2 Å in R_g), which is also reflected in a smaller R_g value for the overall complex (by ∼3 Å). Also, the area of interaction between the components is greater from the present study and seems more realistic. The separation of the centers of mass of the deuterated and nondeuterated components is smaller by ∼10 Å. These differences could reflect differences in sample preparation, but more likely they result from the fact that the significantly higher quality data and larger number of contrast points measured provides for greater accuracy in the current study.

There are a number of important new contributions to our understanding of cardiac troponin structure and function from the current study. Importantly, we have located the cTnT-(198−298) component within the ternary complex, showing it has a compact globular shape and interacts principally with one domain of cTnC, sitting approximately halfway along the extended rod-shaped cTnI. We also have characterized a rather significant conformational change and repositioning of subunits upon phosphorylation of cTnI. Phosphorylation of Ser^{23} and Ser^{24} of cTnI results in the sharp bending of that component, accompanied by a smaller conformational change in the cTnC/cTnT(198−298) component. The models produced by CONTRAST show that in the unphosphorylated state, the cTnC lies along the length of the cTnI/cTnT(198−298) component. Upon phosphorylation, the cTnC/cTnT-(198−298) component remains in contact with the bent end of the cTnI, rotating away from the main axis of the cTnI. Our results suggest that both cTnC and cTnT(198−298) are in contact with cTnI in the general area of the Ser^{23} and Ser^{24} residues.

There have been several studies of the influence of phosphorylation on the interaction between troponin subunits. Interactions between the unphosphorylated cardiac specific N-terminus of cTnI and the regulatory domain of cTnC are thought to stabilize the regulatory domain and favor the conformation in which the hydrophobic cleft formed by the pairs of helices in that domain is open (*7*, *10*, *33*). Phosphorylation of the cardiac specific N-terminus reversed its effects within the regulatory domain (*33*). Mapping of the interactions between the cardiac specific N-terminus and the regulatory domain of cTnC suggests that the cardiac specific N-terminus stabilizes the defunct Ca^{2+} binding site I, thereby increasing the population of open/active regulatory domain conformations (*7*, *34*). These stabilizing regulatory domain interactions are lost upon PKA phosphorylation of cTnI. Fluorescence studies using labeled cTnC have also shown that phosphorylation decreases the Ca^{2+} binding affinity of cTnC (*7*−*9*, *35*) and increases the Ca^{2+} dissociation rates (*36*). Recently, deletion mutagenesis defined the minimal region of the cardiac specific amino terminus of cTnI necessary for stabilizing regulatory domain Ca^{2+} binding to be residues 16−29 (*37*). This result is consistent with earlier studies demonstrating that the binding affinity of the regulatory domain of cTnC for the cTnI(129−166) peptide was reduced in the presence of phosphorylated cTnI-(1−80) as compared to the unphosphorylated fragment (*7*).

Fluorescence studies have also identified conformational changes occurring in cardiac troponin upon PKA phosphorylation of the cardiac specific amino terminus of cTnI (*12*, *13*). The axial ratio of the cTnI decreases producing a more compact structure (*12*). This result is consistent with the bending we observe in cTnI, which results in a broader, shorter structure. A FRET study found that the distance between points in the N- and C-terminus of cTnI decreases by roughly 10 Å (*13*), which is also consistent with the models produced in our study. A surface plasmon resonance study determined that the shape of the cTnI changes in response to phosphorylation, changing from an asymmetrical shape to a more symmetrical one (*14*). The study also found that the Ca^{2+} binding to the complex decreases in response

to the phosphorylation of either or both of the two N-terminal serine residues of cTnI (*14*).

A variety of studies, including photochemical cross-linking, FRET, NMR, and crystallography, have mapped interactions between troponin proteins in binary and ternary troponin complexes. Structural mapping of cTnI using a combination of sulfhydryl reactivity and FRET measurements suggest an open and extended conformation for cTnI (*38*). The binding site for the N-domain of cTnI, corresponding to residues 33−80, has been mapped to the hydrophobic cleft in the C-domain of cTnC (*39*). Similarly, residues 13−29 in sTnI were found to interact with TnC's C-domain in the crystal structure of sTnC/sTnI(1−47), which shows the N-domain of sTnI entering the sTnC C-domain hydrophobic cleft near helices G and H and exiting the cleft near helices E and F (*21*). A similar orientation in cTn would permit the cardiac specific amino terminus, corresponding to residues 1−32, to extend upward toward the N-domain of cTnC. The regulatory domain of cTnI, consisting of residues 147−166, has been shown to interact with the hydrophobic cleft in the N-domain of cTnC (*7*, *40*). In binary cTnC/cTnI complexes, the inhibitory domain of cTnI, consisting of residues 129−147, does not appear to interact specifically with cTnC in the Ca^{2+}-saturated state (*7*). Mapping of the inhibitory and regulatory regions of cTnI in the presence of the N-domain of cTnI suggests that the inhibitory region lies near the linker region in cTnC (*7*, *41*). Recent FRET studies suggest that the inhibitory region adopts an extended structure in the presence of Ca^{2+} (*42*).

The interaction of TnT with the other subunits has also been studied. The binding site for skeletal TnT(160−193) has been localized to the C-domain of sTnC (*43*). Similarly, the binding site for cTnT(171−233) has been localized to the C-domain of cTnC, both in the presence and in the absence of cTnI(33−80) (Finley and Rosevear, unpublished). Binding of TnT to TnI has been suggested to occur through a coiled−coil interaction involving heptad repeats in both proteins (*44*−*46*). This would localize the cTnT binding site to residues 91−143 in cTnI and the cTnI binding site to residues 248−274 in cTnT. A preliminary report on the crystal structure of skeletal TnT2 bound to sTnC and sTnI showed the coiled-coil region of sTnT interacting with the coiled−coil region of sTnI (*47*).

Using the results of the previous studies, we can construct a model of the relative orientations of the cTn subunits in our consensus envelope models. The peanut-shaped cTnC would be orientated such that the lower lobe of the consensus envelope represents the C-domain (Figures 7 and 10). As a consequence of the antiparallel arrangement between cTnC and cTnI, the lower portion of the rodlike cTnI consensus envelope would represent the N-domain of cTnI (Figures 8 and 9). The upper lobe of the cTnC consensus envelope is assigned to the N- or regulatory domain of cTnC. The N-domain of cTnC would then be positioned in a region of the cTnI consensus envelope comprising the regulatory region. The remaining C-terminal portion of cTnI, comprising residues 167−211, is assigned to the free end of the rodlike structure. The TnT(198−298) was inferred to be the extra globular domain located near the center of the cTnI component (Figure 7B). It is possible that cTnT(198−298) is somewhat elongated and orientated approximately 90° with respect to the long axis of cTnC (Figure 10B), but the consensus envelope does not contain enough detail to say this conclusively. Such an arrangement is consistent with previous interaction studies of TnT binding to TnC and TnI. A region of cTnT(198−298) is believed to interact with the heptad repeat located near the middle of the rodlike cTnI, which is consistent with our model. In addition, cTnT(198−298) contains binding sites for both the N- and the C-domains of cTnC, with the N-terminal portion of cTnT(198−298) interacting exclusively with the C-domain of cTnC.

On the basis of our arguments for the relative orientations of the Tn subunits, we can speculate on the mechanism by which bisphosphorylation of the cardiac specific amino terminus modifies the Ca^{2+} sensitivity and structure of the complex. In the unphosphorylated state, the cardiac specific amino terminus of cTnI, corresponding to residues 1−32, interacts with the regulatory domain of cTnC. Bisphosphorylation or mutation of cTnI Ser^{23} and Ser^{24} to Asp results in a loss of these interactions (*10*, *33*). This results in a destabilization of the regulatory domain of cTnC (*7*, *39*) that may alter its Ca^{2+}-binding properties.

Bisphosphorylation of cTnI induces a rotation of the cTnI N-domain away from the main axis of cTnI (Figures 10 and 11). One possible mechanism by which phosphorylation could induce a rotation of the N-terminal portion of cTnI involves a direct interaction of the cardiac specific amino terminus with a region of cTnI C-terminal to residues 33−80 comprising the N-domain. This hypothesis is consistent with the observation that phosphorylation of the cardiac specific amino terminus induces a 10−12 Å movement toward cTnI (*48*). Alternatively, the bisphosphorylated cardiac specific amino terminus could interact with a region of cTnT(198−298). The cTnC/cTnT(198−298) component remains essentially unaltered upon cTnI phosphorylation (Figures 8A and 9A), so it seems most likely that the phosphorylated cardiac specific amino terminus releases its interaction with the regulatory domain of cTnC and primarily interacts with TnT. The concerted movement of the cTnC/cTnT(198−298) component would occur, at least in part, because of the high affinity interaction between the C-domain of cTnC and the N-domain of cTnI.

The shape changes induced by phosphorylation of cTnI are reminiscent of a lever action. Lever actions are thought to be important in transmission of the Ca^{2+} signal in muscle contraction (*49*). Our results suggest that a lever action may also be involved in the modulation of that signal via phosphorylation.

REFERENCES

1. Holmes, K. C. (1997) *Curr. Biol. 7*, R112−R118.
2. Cook, R. (1997) *Physiol. Rev. 77*, 671−697.
3. Gergely, J. (1998) *Adv. Exp. Med. Biol. 453*, 169−176.
4. Perry, S. V. (1999) *Mol. Cell Biochem. 190*, 9−32.
5. Van Eerd, J. P., and Takahashi, K. (1975) *Biochem. Biophys. Res. Commun. 64*, 122−127.
6. Moir, A. J., Solaro, R. J., and Perry, S. V. (1980) *Biochem. J. 185*, 505−513.
7. Abbott, M. B., Dong, W. J., Dvoretsky, A., DaGue, B., Caprioli, R. M., Cheung, H. C., and Rosevear, P. R. (2001) *Biochemistry 40*, 5992−6001.
8. Robertson, S. P., Johnson, J. D., Holroyde, M. J., Kranais, E. G., Potter, J. D., and Solaro, R. J. (1982) *J. Biol. Chem. 257*, 260−263.
9. Zhang, R., Zhao, J., and Potter, J. D. (1995) *J. Biol. Chem. 270*, 30773−30780.

10. Gaponenko, V., Abusamhadneh, E., Abbot, M. B., Finley, N., Gasmi-Seabrook, G., Solaro, R. J., Rance, M., and Rosevear, P. R. (1999) *J. Biol. Chem. 274*, 16681−16684.
11. Finley N., Abbott, M. B., Abusamhadneh, E., Gaponenko, V., Dong, W., Gasmi-Seabrook, G., Howarth, J. W., Rance, M., Solaro, R. J., Cheung, H. C., and Rosevear, P. R. (1999) *FEBS Lett. 453*, 107−112.
12. Dong, W.-J., Chandra, M., Xing, J., Solaro, R. J., and Cheung, H. C. (1997) *Biochemistry 36*, 6745−6753.
13. Dong, W.-J., Chandra, M., Xing, J., She, M., Solaro, R. J., and Cheung, H. C. (1997) *Biochemistry 36*, 6754−6761.
14. Reiffert, S. U., Jaquet, K., Heilmeyer, L. M. G., Jr., and Herberg, F. W. (1998) *Biochemistry 37*, 13516−13525.
15. Heller, W. T., Abusamhadneh, E., Finley, N., Rosevear, P. R., and Trewhella, J. (2002) *Biochemistry 41*, 15654−15663.
16. Stone, D. B., Timmins, P. A., Schneider, D. K., Krylova, I., Ramos, C. H. I., Reinach, F. C., and Mendelson, R. A. (1998) *J. Mol. Biol. 281*, 689−704.
17. Olah, G. A., Rokop, S. E., Wang, C.-L. A., Blechner, S. L., and Trewhella, J. (1994) *Biochemistry 33*, 8233−8239.
18. Olah, G. A., and Trewhella, J. (1994) *Biochemistry 33*, 12800−12806.
19. Sundaralingam, M., Bergstrom, R., Strasburg, G., Rao, S. T., Roychowdhury, P., Greaser, M., and Wang, B. C. (1985) *Science 227*, 945−948.
20. Dvoretsky, A., Abusamhadneh, E., Howarth, J., and Rosevear, P. R. (2002) *J. Biol. Chem. 277*, 38565−38570.
21. Vassylyev, D. G., Takeda, S., Wakatsuki, S., Maeda, K., and Maeda, Y. (1998) *Proc. Natl. Acad. Sci. U.S.A. 95*, 4847−4852.
22. Tung, C. S., Wall, M. E., Gallagher, S. E., and Trewhella, J. (2000) *Protein Sci. 9*, 1312−1326.
23. Heidorn, D. B., and Trewhella, J. (1988) *Biochemistry 27*, 909−915.
24. Krigbaum, W. R., and Kugler, F. R. (1970) *Biochemistry 9*, 1216−1223.
25. Information on the D22 instrument at the ILL can be found at http://whisky.ill.fr/YellowBook/D22/.
26. Information on data reduction at the ILL can be found at http://www.ill.fr/data_treat/sanstreat.html.
27. Guinier, A. (1939) *Ann. Phys. (Paris) 12*, 161−237.
28. Moore, P. B. (1980) *J. Appl. Crystallogr. 13*, 168−175.
29. Ibel, K., and Stuhrmann, H. B. (1975) *J. Mol. Biol. 93*, 255−265.
30. Bevington, P. R. (1969) *Data Reduction and Error Analysis for the Physical Sciences*, New York, McGraw-Hill.
31. Hjelm, R. P., Jr., Baldwin, J. P., and Bradbury, E. M. (1978) in *Methods in Cell Biology, Vol. 18; Chromatin and Chromosomal Protein Research, Part 3* (Stein, G., Stein, J., and Kleinsmith, L. J., Eds.) Academic Press, New York, London.
32. Krudy, G. A., Kleerhoper, Q., Guo, X., Howarth, J. W., Solaro, R. J., and Rosevear, P. R. (1994) *J. Biol. Chem. 269*, 23731−23735.
33. Abbott, M. B., Gaponenko, V., Abusamhadneh, E., Finley, N., Li, G., Dvoretsky, A., Rance, M., Solaro, R. J., and Rosevear, P. R. (2000) *J. Biol. Chem. 275*, 20610−20617.
34. Abusamhadneh, E., Abbott, M. B., Dvoretsky, A., Finley, N., Sasi, S., and Rosevear, P. R. (2001) *FEBS Lett. 506*, 51−54.
35. Liao, R., Wang, C.-K., and Cheung, H. C. (1994) *Biochemistry 33*, 12729−12734.
36. Dong, W.-J., Wang, C.-K., Gordon, A. M., Rosenfeld, S. S., and Cheung, H. C. (1997) *J. Biol. Chem. 272*, 19229−19235.
37. Ward, D. G., Cornes, M. P., and Trayer, I. P. (2002) *J. Biol. Chem. 277*, 41795−41801.
38. Dong, W.-J., Xing, M., Chandra, M., Solaro, J., and Cheung, H. C. (2000) *Proteins 41*, 438−447.
39. Gasmi-Seabrook, G. M., Howarth, J. W., Finley, N., Abusamhadneh, E., Gaponenko, V., Brito, R. M., Solaro, R. J., and Rosevear, P. R. (1999) *Biochemistry 38*, 8313−8322.
40. Li, M., Spyracopoulos, L., and Sykes, B. D. (1999) *Biochemistry 38*, 8289−8298.
41. Luo, Y., Wu, J.-L., Li, B., Langsetmo, K., and Gergely, J. (2000) *J. Mol. Biol. 296*, 899−910.
42. Dong, W.-J., Xing, J., Robinson, J. M., and Cheung, H. C. (2001) *J. Mol. Biol. 314*, 51−61.
43. Blumenschein, T. M., Tripet, B. P., Hodges, R. S., and Sykes, B. D. (2002) *J. Biol. Chem. 276*, 36606−36612.
44. Stefancsik, R., Jha, P. K., and Sarkar, S. (1998) *Proc. Natl. Acad. Sci. U.S.A. 95*, 957−962.
45. Pearlstone, J. R., and Smillie, L. B. (1985) *Can. J. Biochem. 63*, 212−218.
46. Malnic, B., Farah, C. S., and Reinach, F. C. (1998) *J. Biol. Chem. 273*, 10594−10601.
47. Takeda, S., Yamashita, A., Maeda, K., and Maeda, Y. (2002) *Biophys. J. 82*, 170a.
48. Dong, W.-J., Chandra, M., Xing, J., She, M., Solaro, J. R., and Cheung, H. C. (1997) *Biochemistry 36*, 6754−6761.
49. Narita, A., Yasunaga, T., Ishikawa, T., Mayanagi, K., and Wakabayashi, T. (2001) *J. Mol. Biol. 308*, 241−261.

BI0341509